Inorganic Chemistry

Article

pubs.acs.org/IC

Wells–Dawson Cages as Molecular Refrigerants

Eufemio Moreno Pineda, Floriana Tuna, Yan-Zhen Zheng,† Richard E. P. Winpenny,* and Eric J. L. McInnes*

School of Chemistry and Photon Science Institute, The University of Manchester, Oxford Road, Manchester M13 9PL, U.K.

Supporting Information

ABSTRACT: Five clusters with the general formula $[Ni_6Gd_6(\mu_3\text{-}OH)_2(\mu_2\text{-}OAc)_2(O_3PR)_6(O_2C^tBu)_{16}]$, where R = methyl (**1**), phenyl (**2**), *n*-hexyl (**3**), benzyl (**4**), *n*-octyl (**5**), have been prepared. All of the clusters have a $\{Ni_6Gd_6P_6\}$ core that can be related to the Wells–Dawson ion. We have also prepared analogues where the gadolinium is replaced with diamagnetic yttrium: $[Ni_6Y_6(\mu_3\text{-}OH)_2(\mu_2\text{-}OAc)_2(O_3PR)_6(O_2C^tBu)_{16}]$ (R = methyl (**6**), *n*-hexyl (**7**), benzyl (**8**), *n*-octyl (**9**)), allowing the magnetic exchange within the $\{Ni_3\}$ units to be analyzed by modeling as the sum of two noninteracting isosceles triangles. The variation in the magnetic entropy changes for magnetization ($-\Delta S_M$) among compounds **1**–**5** could be attributed not only to the molecular weight of the compounds but also to intramolecular magnetic interactions.

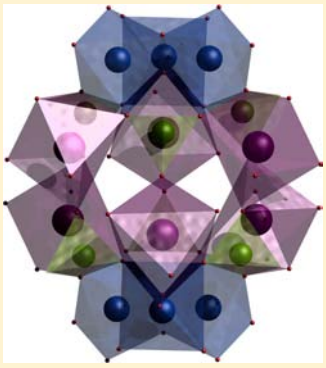

INTRODUCTION

Paramagnetic cage complexes, sometimes called molecular nanomagnets (MNMs), have been extensively studied due to their interesting physics and the possibility of exploiting their magnetic behavior in technological applications.[1] The most explored family of MNMs are the single-molecule magnets (SMMs), where the molecules show slow relaxation of magnetization. Other applications that have been proposed for MNMs include quantum information processing, spintronics, and magnetic refrigerants. Magnetic refrigerants are based on the magnetocaloric effect (MCE), where an adiabatic demagnetization process leads to cooling. MNMs can be used to achieve very low (sub-Kelvin) temperatures.[2] Good candidate molecules have negligible magnetic anisotropy but a high-spin ground state or at least a highly degenerate set of low-lying states that can saturate in applied field. Ferromagnetic interactions between the metal centers can be favorable, since this gives rise to faster magnetization in low applied fields. The frequent observation of ferromagnetic interactions in 3d–4f mixed-metal cages has led to recent studies of such compounds for this application, often involving the isotropic Gd^{III} ion ($S = {}^7/_2$) to obtain high magnetic entropy changes ($-\Delta S_M$) on (de)magnetization.[3]

We, and others, have recently reported the use of phosphonates ($R\text{-}PO_3^{2-}$) to make 3d–4f cage complexes.[4] The tendency of metal phosphonates to form insoluble polymeric materials can be controlled by the addition of coligands or by the use of bulky R groups. Our first study with nickel lanthanides produced a $\{Ni_6Ln_6P_6\}$ rugby-ball-shaped molecule[4c] that showed weak ferromagnetic coupling within the $\{Ni_3\}$ moiety with consequent high MCE. One important characteristic of molecules for MCE is the molecular weight, because ultimate exploitation depends on the mass (or density) of the material. Herein we report systematic variations of the $\{Ni_6Ln_6P_6\}$ cage by changing the phosphonate. We find that the metal core is robust and insensitive to modification of the R group, but there are subtle changes in the MCE parameters beyond those predicted simply from mass changes. Diamagnetic lanthanide analogues are prepared to quantify changes in the magnetic interactions within the cages across the series.

EXPERIMENTAL SECTION

Materials and Physical Measurements. All reagents and solvents were purchased from Aldrich Chemicals and used without further purification. $[Ni_2(\mu_2\text{-}OH_2)(O_2C^tBu)_4(HO_2C^tBu)_4]$ and $[Ln_2(O_2C^tBu)_6(HO_2C^tBu)_6]$ (Ln = Gd, Y) were prepared by reported methods.[5,6] Analytical data and yields are given in Table 1.

Synthesis. Cages **1**–**9** were synthesized under similar conditions. $[Ni_2(\mu_2\text{-}OH_2)(O_2C^tBu)_4(HO_2C^tBu)_4]$ (0.1 g, 0.1 mmol), $[Gd_2(O_2C^tBu)_6(HO_2C^tBu)_6]$ (0.075 mmol), RPO_3H_2 (R = methyl, phenyl, *n*-hexyl, benzyl, *n*-octyl) (0.1 mmol), and triethylamine (Et_3N) (0.1 mL, 1 mmol) in acetonitrile (MeCN) (8 mL) were stirred at room temperature for 5 min. The resulting slurry was transferred into a 10 mL Teflon-lined autoclave, which was heated to 150 °C for 12 h and then cooled to room temperature at a rate of 0.05 °C min^{-1}. Yellow X-ray-quality crystals were obtained for methyl (**1**), phenyl (**2**), *n*-hexyl (**3**), benzyl (**4**), and *n*-octyl (**5**) phosphonic acids directly from the autoclave. Similar conditions of reactions but replacing the $[Gd_2(O_2C^tBu)_6(HO_2C^tBu)_6]$ source with $[Y_2(O_2C^tBu)_6(HO_2C^tBu)_6]$ yielded analogous clusters for methyl (**6**), *n*-hexyl (**7**), benzyl (**8**) and *n*-octyl (**9**) phosphonic acid. Attempts to synthesize the Y analogue of complex **2** $\{Ni_6Gd_6P_6\}$ (R = phenyl) were unsuccessful.

Crystallography. Single-crystal X-ray diffraction measurements for **1**–**4** were carried out on a Bruker SMART CCD diffractometer with Mo Kα radiation (λ = 0.71073 Å) at 100 K. The data collection of **5**–**7**

Received: September 10, 2013
Published: November 12, 2013

   dx.doi.org/10.1021/ic402296t | *Inorg. Chem.* 2013, 52, 13702–13707

Table 1. Elemental Analysis and Yield (%) for Compounds 1−9

			elemental analysis: found (calcd)					
compd	formula	yield[a]	C	H	N	Ni	Ln	P
1	$[Ni_6Gd_6(\mu_3\text{-}OH)_2(OAc)_2(O_3PMe)_6(O_2C^tBu)_{16}]$	35	30.12 (29.76)	4.60 (4.77)	0 (0)	9.54 (9.69)	26.06 (25.98)	5.18 (5.12)
2	$[Ni_6Gd_6(\mu_3\text{-}OH)_2(OAc)_2(O_3PPh)_6(O_2C^tBu)_{16}]\cdot 2MeCN$	20	36.04 (36.45)	4.82 (4.69)	0.87 (0.68)	8.34 (8.62)	23.29 (23.1)	4.69 (4.55)
3	$[Ni_6Gd_6(\mu_3\text{-}OH)_2(OAc)_2(O_3PHex)_6(O_2C^tBu)_{16}]\cdot 2MeCN$	46	35.76 (36.02)	5.86 (5.80)	0.74 (0.68)	8.69 (8.52)	23.11 (22.82)	4.75 (4.50)
4	$[Ni_6Gd_6(\mu_3\text{-}OH)_2(OAc)_2(O_3PCH_2Ph)_6(O_2C^tBu)_{16}]\cdot 2MeCN$	77[b]	37.90 (37.85)	4.88 (4.93)	1.25 (1.32)	8.21 (8.28)	22.14 (22.19)	4.46 (4.37)
5	$[Ni_6Gd_6(\mu_3\text{-}OH)_2(OAc)_2(O_3POct)_6(O_2C^tBu)_{16}]\cdot 2MeCN$	53	38.17 (37.96)	5.89 (6.14)	0.56 (0.65)	7.98 (8.18)	21.83 (21.92)	4.37 (4.32)
6	$[Ni_6Y_6(\mu_3\text{-}OH)_2(OAc)_2(O_3PMe)_6(O_2C^tBu)_{16}]\cdot 2MeCN$	28	34.00 (34.17)	5.49 (5.43)	0.81 (0.85)	10.51 (10.66)	15.98 (16.14)	5.39 (5.62)
7	$[Ni_6Y_6(\mu_3\text{-}OH)_2(OAc)_2(O_3PHex)_6(O_2C^tBu)_{16}]\cdot 2MeCN$	49	39.60 (39.99)	6.52 (6.44)	0.73 (0.75)	9.25 (9.45)	13.78 (14.32)	4.99 (4.98)
8	$[Ni_6Y_6(\mu_3\text{-}OH)_2(OAc)_2(O_3PCH_2Ph)_6(O_2C^tBu)_{16}]\cdot 4MeCN$	70[b]	41.63 (41.89)	5.51 (5.46)	1.33 (1.46)	9.12 (9.16)	13.79 (13.88)	4.81 (4.84)
9	$[Ni_6Y_6(\mu_3\text{-}OH)_2(OAc)_2(O_3POct)_6(O_2C^tBu)_{16}]\cdot 2MeCN$	54	42.20 (41.97)	6.52 (6.78)	0.63 (0.72)	9.15 (9.04)	13.83 (13.70)	4.93 (4.77)

[a]Calculated on the basis of the lanthanide pivalate starting material. [b]Calculated on the basis of the lanthanide phosphonate starting material.

Table 2. Crystallographic Information for Clusters 1−9

	1	**2**	**3**	**4**	**5**
chem formula	$C_{90}H_{170}Gd_6Ni_6P_6O_{56}\cdot 2CH_3CN$	$C_{120}H_{182}Gd_6Ni_6P_6O_{56}\cdot 2CH_3CN$	$C_{120}H_{230}Gd_6Ni_6P_6O_{56}$	$C_{126}H_{184}Gd_6Ni_6P_6O_{56}\cdot 4CH_3CN$	$C_{132}H_{256}Gd_6Ni_6P_6O_{56}\cdot 4CH_3CN$
fw	3711.94	4084.33	4050.61	4252.62	4383.13
cryst syst	triclinic	monoclinic	triclinic	monoclinic	triclinic
space group	$P\bar{1}$	$P2_1/n$	$P\bar{1}$	$P2_1/n$	$P\bar{1}$
a/Å	15.4495(5)	18.3716(8)	16.5791(4)	18.8556(14)	16.4562(4)
b/Å	16.0319(5)	20.4859(8)	20.5132(4)	16.0904(12)	17.6336(4)
c/Å	16.3513(6)	21.8809(9)	25.5694(5)	28.384(2)	18.5683(4)
α/deg	104.512(3)	90.00	84.2046(17)	90.00	79.888(2)
β/deg	101.152(3)	94.926(4)	89.3037(18)	94.9300(10)	70.274(2)
γ/deg	100.934(3)	90.00	89.3726(18)	90.00	68.785(2)
V/Å^3	3723.9(2)	8204.6(6)	8650.4(3)	8579.68	4719.5(2)
Z	1	2	2	2	1
ρ_{calcd}/g cm^{-3}	1.655	1.653	1.555	1.646	1.542
T/K	104(2)	100.15	100.15	100.00	100.15
μ(Mo Kα)/mm^{-1}	3.511	3.195	3.029	3.060	2.783
R1($I > 2\sigma(I)$)[a]	0.0509	0.0916	0.0841	0.0464	0.0574
wR2[a]	0.1028	0.1854	0.1822	0.1121	0.1298

	6	**7**	**8**	**9**
chem formula	$C_{94}H_{176}N_2Ni_6O_{56}P_6Y_6\cdot 2CH_3CN$	$C_{120}H_{228}Ni_6O_{56}P_6Y_6$	$C_{134}H_{208}N_4Ni_6O_{56}P_6Y_6\cdot 4CH_3CN$	$C_{132}H_{248}Ni_6O_{56}P_6Y_6$
fw	3301.90	3640.57	3842.48	3806.86
cryst syst	triclinic	triclinic	monoclinic	triclinic
space group	$P\bar{1}$	$P\bar{1}$	$P2_1/n$	$P\bar{1}$
a/Å	15.5870(7)	16.6447(4)	18.8806(9)	16.2833(9)
b/Å	16.0533(7)	20.5345(4)	16.0529(7)	17.5109(15)
c/Å	16.3662(7)	25.1562(6)	28.2345(13)	18.3682(9)
α/deg	104.895(4)	84.0060(18)	90.00	81.023(6)
β/deg	101.521(4)	88.9737(18)	94.8310(10)	70.241(5)
γ/deg	100.704(4)	89.5098(16)	90.00	69.087(7)
V/Å^3	3754.4(3)	8549.6(3)	8527.1(7)	4600.6(6)
Z	1	2	2	1
ρ_{calcd}/g cm^{-3}	1.460	1.414	1.497	1.374
T/K	128.35(10)	128.40(10)	100(2)	150.03(18)
μ(Mo Kα)/mm^{-1}	3.162	2.784	2.797	2.590
R1($I > 2\sigma(I)$)[a]	0.0733	0.0678	0.0576	0.0931
wR2[a]	0.1511	0.1708	0.1435	0.2279

[a]$R1 = ||F_o| - |F_c||/|F_o|$; $wR2 = [w(|F_o| - |F_c|)^2/w|F_o|^2]^{1/2}$.

dx.doi.org/10.1021/ic402296t | Inorg. Chem. 2013, 52, 13702−13707

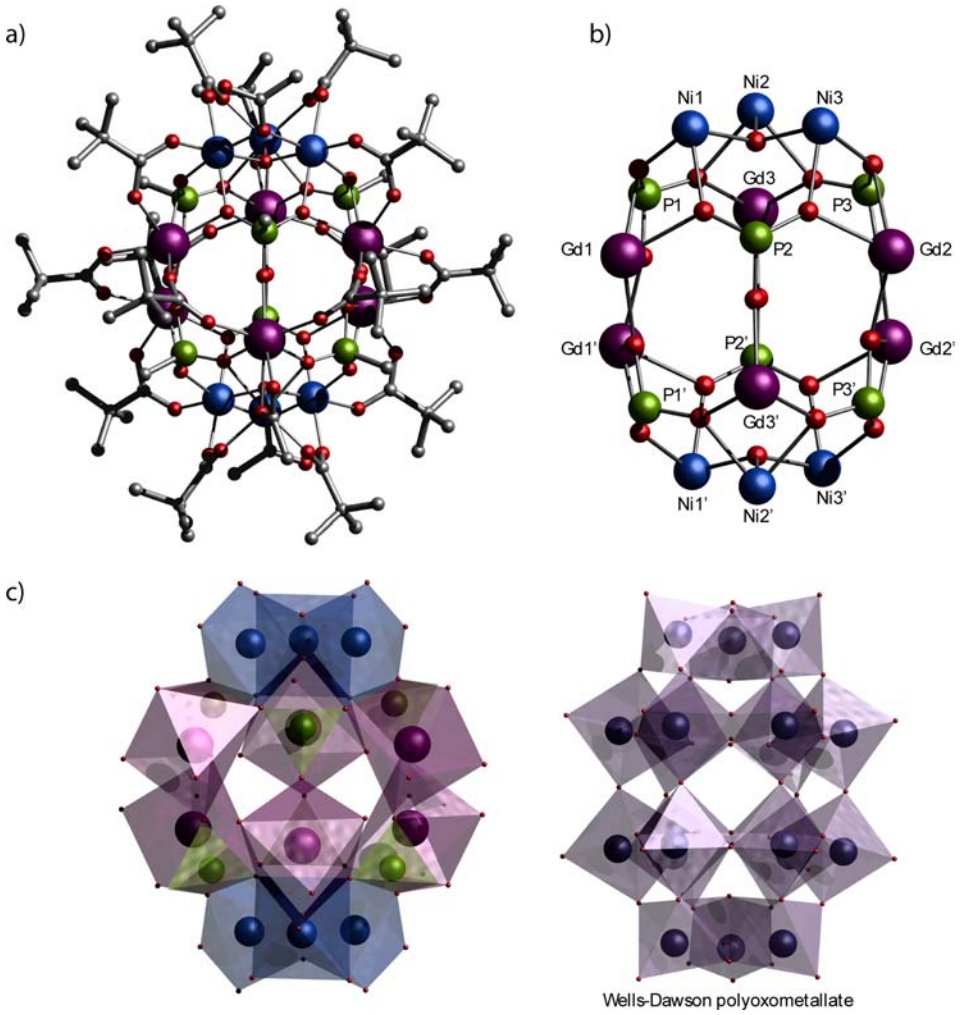

Figure 1. (a) Crystal structure and (b) $\{Ni_6Ln_6P_6\}$ core of **1**-**9**. Scheme: Gd/Y, purple; Ni, blue; P, green; O, orange; C, gray; H omitted for clarity. (c) Polyhedral view of $\{Ni_6Ln_6P_6\}$ core and comparison with the $\{M_{18}\}$ Wells-Dawson core.

was carried out on Agilent SUPERNOVA diffractometer with Mo Kα radiation (λ = 0.71073 Å) at 150 K. Data reduction and unit cell refinement were performed with Crysallis software. The structures were solved by direct methods using SHELXS-97 and were refined by full-matrix least-squares methods using Olex2.[7] Crystal data and refinement parameters are given in Table 2. Selected bond lengths and angles are given in the Supporting Information. CCDC deposition numbers: 958734–958740, 805050, and 805052.

Magnetic Measurements. The magnetic properties of polycrystalline samples of **1**–**9** were measured with a Quantum Design MPMS-XL7 SQUID magnetometer. The samples were ground, placed in a gel capsule, and fixed with a small amount of eicosane to avoid movement during the measurement. The data were corrected for the diamagnetism from the gel capsule and the eicosane with the diamagnetic contribution from the complexes calculated from Pascal constants.

RESULTS AND DISCUSSION

Synthetic Description. Solvothermal synthesis has proved to be effective in producing high-nuclearity polymetallic cages,[8] and we have previously reported 3d–4f phosphonate cages synthesized through this technique.[4] Here we found optimal conditions for synthesis of the $\{Ni_6Ln_6P_6\}$ cages to be 150 °C in MeCN, giving yields obtained between 20 and 60%.

Structure. The compounds crystallize in two different space groups, $P\bar{1}$ (**1**, **3**, **5**–**7**, and **9**) and $P2_1/n$ (**2**, **4**, and **8**); however, there is little difference between the molecular structures and the description below serves for all molecules. In each case the cage lies on an inversion center. The cage can be described as a rugby ball (Figure 1 and Figure S1 (Supporting Information)). The two ends of the rugby ball are capped by a $\{Ni_3(\mu_3\text{-OH})\}$ triangle, in which the μ_3-OH group is displaced ca. 0.47(2)–0.49(2) Å out of the $\{Ni_3\}$ plane (see Table S1 (Supporting Information)). There are two chemically distinct Ni···Ni edges (Figure S7 (Supporting Information)). To describe the binding modes of the polynucleating ligands, we use Harris notation,[14] $X.Y_1Y_2Y_3$, where X is the overall number of metals bound by the whole ligand, and each value of Y refers to the number of metal atoms attached to the different donor atoms (Figure S2 (Supporting Information)). The Ni1···Ni2 and Ni2···Ni3 edges are each bridged by a 2.11 pivalate (exo to the cage) and one arm of a 5.222 phosphonate (P1 or P3), also bridging to three Ln ions. The Ni1···Ni3 edge is bridged by a 2.20 acetate (exo to the cage) and a 5.221 phosphonate (P2). Hence, the $\{Ni_3\}$ triangles approximate very closely isosceles triangles with a short Ni1···Ni3 edge (Figure S7 (Supporting Information)). Note that although acetate was not added to the reaction, hydrolysis of MeCN under solvothermal conditions is known[9] and in situ formation of carboxylates in solvothermal cage synthesis is well established.[4g,10] Deliberate addition of acetate does not improve the yield of crystalline material, and we have

dx.doi.org/10.1021/ic402296t | Inorg. Chem. 2013, 52, 13702–13707

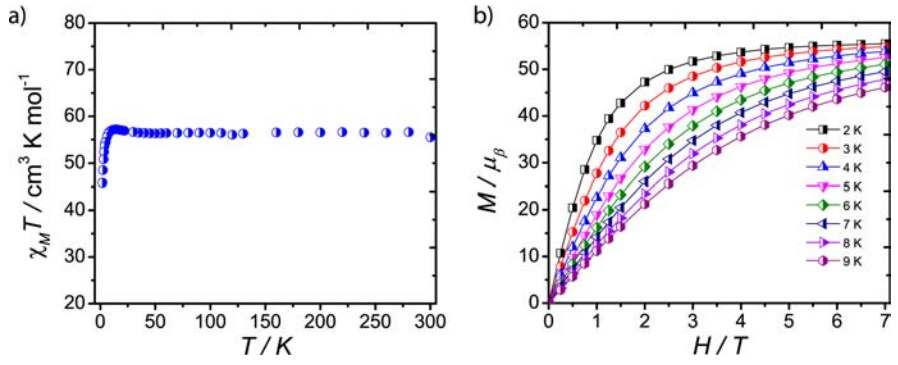

Figure 2. Magnetic studies of **1**: (a) $\chi_M T$ vs T measured in a 1 kG applied magnetic field and (b) M vs H at the temperatures indicated.

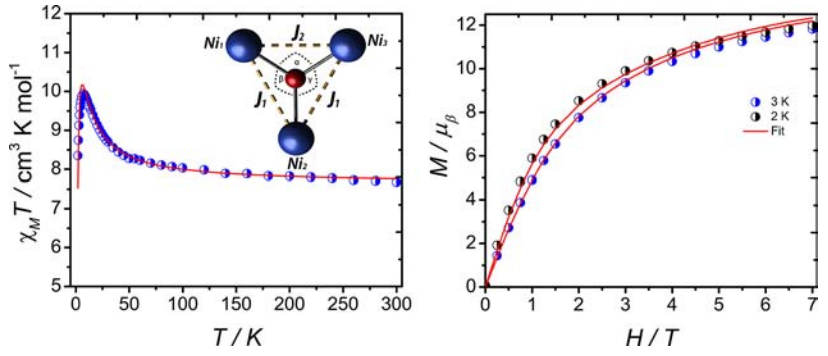

Figure 3. Magnetic measurements on compound **6**: (left) $\chi_M T$ vs T measured in a 1 kG field; (right) M vs H at the temperatures indicated. Red lines are the best simultaneous fits to Hamiltonian (1).

also been unable to include other bridging ligands in the structure. The bridging between the Ni and Ln ions is completed by three pivalates using either the 2.11 or the 2.21 coordination modes.

The alternating arrangement of the Ln and P atoms forms a $\{Ln_3P_3\}$ six-membered ring, which connects to its centrosymmetric-related counterpart through six 2.11 pivalates. The Gd···Gd separations within the $\{Gd_3P_3\}$ six-membered rings in **1**−**5** fall into the range 6.05−6.57 Å, whereas those between the $\{Gd_3P_3\}$ rings are shorter, in the range 3.9−4.9 Å. In the yttrium cages **6**−**9** the analogous Y···Y ranges are 5.9−6.50 and 3.138−4.60 Å, respectively. If the P atoms are treated as part of the core of these cages, the resulting $\{Ni_6Ln_6P_6\}$ units resemble the Wells−Dawson polyoxometalate (Figure 1c right). This complements the paramagnetic "Keggin" ions that have been reported.[13]

Magnetism. The magnetic behavior of **1**−**9** has been studied on polycrystalline samples (Figure 2 and Figure S3 (Supporting Information)). At room temperature **1**−**5** all have $\chi_M T$ values (where χ_M is the molar magnetic susceptibility) close to the sum of the calculated value (54.1 emu K mol^{-1}) for six $S = 1$, $g = 2.2$ and six $S = {}^7/_2$, $g = 2.00$ centers. Upon cooling, $\chi_M T$ changes little down to about 50 K, before increasing slowly to a maximum at around 15 K. Magnetization (M) versus applied field (H) measurements at low temperature all saturate at around 55 μ_B (Figure 2b and Figures S3 and S5 (Supporting Information)), consistent with the maximum possible value for full alignment of spins.

Compounds **6**−**9** were studied in order to understand the magnetic interactions in and between the $\{Ni_3\}$ moieties. The behaviors of the four compounds are very similar (Figure 3 and Figure S4 (Supporting Information)). At room temperature the $\chi_M T$ value is slightly above that calculated for six $S = 1$ centers with $g = 2.2$ (7.26 cm^3 K mol^{-1}), with observed values of 7.8, 8.2, 7.9, and 7.9 cm^3 K mol^{-1} for **6**−**9**, respectively. In each case the $\chi_M T$ value increases smoothly to a maximum at near 10 K, before falling at lower temperatures. Low-temperature M *vs* H studies show a steady increase up to 7 T, tending toward saturation at slightly above 12 μ_B (Figure 3 and Figures S4 and S5 (Supporting Information)).

The behavior of **6**, **7** and **9** was modeled using PHI software[11] with Hamiltonian (1), fitting $\chi_M T$ vs T and M vs H simultaneously. Data and fits for **8** were reported previously.[4c]

$$H = -2J_1(\hat{S}_1\hat{S}_2 + \hat{S}_2\hat{S}_3) - 2J_2(\hat{S}_1\hat{S}_3) + D\sum_{i=1}^{3} S_{iz}{}^2 + g\mu_B H \sum_{i=1}^{3} \hat{S}_i \quad (1)$$

Hamiltonian (1) assumes an isosceles triangle (see above) with the first term being the isotropic exchange interaction between Ni(1)···Ni(2) and Ni(2)···Ni(3) and the second term that between Ni(1)···Ni(3), the chemically unique edge (Figure 3, inset). The third and fourth terms are the axial zero field splitting (ZFS) and Zeeman terms, respectively, of each Ni center. No meaningful simultaneous fits to $\chi_M T$ vs T and M vs H could be obtained without inclusion of the ZFS terms or with an equilateral model. For simplicity the ZFSs are taken as collinear and identical for all three Ni ions. Best statistical fits (Figure 3) to the experimental data were found using the parameters in Table 3.

The two $\{Ni_3\}$ triangles are treated as noninteracting, i.e. the results of Hamiltonian (1) are simply multiplied by a factor of 2. In each case we find two ferromagnetic and one

dx.doi.org/10.1021/ic402296t | Inorg. Chem. 2013, 52, 13702−13707

Table 3. Magnetic Data for 1−9

	R group in RPO_3^{2-}				
	Me	Ph	hexyl	CH_2Ph	octyl
Gd complex	**1**	**2**	**3**	**4**	**5**
Y complex	**6**		**7**	**8**	**9**
J_1/cm^{-1} (for Y complex)	2.4		4.8	2.83	4.5
J_2/cm^{-1} (for Y complex)	−1.0		−3.5	−1.18	−2.7
D/cm^{-1} (for Y complex)	6.2		4.3	5.7	5.8
g (for Y complex)	2.28		2.32	2.28	2.27
$-\Delta\sum_\mu/J\ kg^{-1}\ K^{-1}$ (for Gd complex)[a]	32	27.9	28.2	26.5	26.6
$-\Delta\sum_\mu/J\ mol^{-1}\ K^{-1}$ (for Gd complex)[a]	116.1	111.7	114.2	105.5	115.4

[a]Calculated for a ΔH = 0−7 T, at 3 K.

antiferromagnetic interaction within the $\{Ni_3\}$ triangles. The unique interaction (J_2) is presumably for the significantly shorter Ni(1)···Ni(3) edge ,which has a correspondingly much smaller Ni(1)−O−Ni(3) angle of ca. 104−105°: cf. the 118−121° angles found for the other two edges (Table 4).

Table 4. Ni(i)···OH···Ni(j) Angles (deg) (See Figure 3 Inset) in the $\{Ni_3\}$ Moiety

	α	β	γ
methyl	104.4(2)	119.2(2)	119.5(2)
benzyl	104.2(1)	120.4(2)	118.7(2)
hexyl[a]	103.50(4)	119.3(4)	119.93(4)
octyl	104.2(3)	120.8(3)	118.0(3)

[a]Average distance of the two molecules in the asymmetric unit cell.

The magnitudes of D obtained for **6**−**9** seem at first surprisingly large for $\{NiO_6\}$ coordination environments (Table 3). However, these environments are far from homoleptic, and the ligand fields at Ni are likely to be strongly axial, dominated by the short Ni···μ_3-OH interactions of 1.960(6)−2.009(7) Å, with the remaining O donors from phosphonate and carboxylate in the range 1.975(8)−2.229(3) Å (see Figure S7 and Table S1 (Supporting Information)). Even small deviations from regular octahedral environments can give rise to significant ZFS values for Ni^{II}.[12]

In order to understand the interaction between Ni···Gd and Gd···Gd within the clusters, the magnetization curve for six noninteracting Gd^{III} ions was calculated using the Brillouin function and added to the experimental data for the $\{Ni_6Y_6P_6\}$ cages. These curves were then compared with the experimental data for the analogous $\{Ni_6Gd_6P_6\}$ compounds (Figure 4). For cages **3**−**5** the curves agree well; hence, the Ni···Gd interactions must be negligible. However, the magnetization curve of **1** is slightly higher than that calculated from **6** plus six Gd^{III}. This suggests that weak ferromagnetic Ni···Gd interactions are operating in **1** but not in **3**−**5**.

The rapid magnetization observed for the $\{Ni_6Gd_6P_6\}$ cages, due to the ferromagnetic coupling, with achievement of full spin alignment, led us to study the magnetic entropy changes for these processes (Table 3 and Figure S6 (Supporting Information)). The maximum magnetic entropy change value *per mass* was achieved for the methylphosphonate derivative **1**, with a value of 32 J kg^{-1} K^{-1}: this is entirely predictable, as **1** has the lowest molecular weight. However, this does not appear to be the only factor, as the increase is greater than predicted purely on the grounds of mass change.

Comparing the *molar* magnetic entropy change for each case, we can clearly see that the molar magnetic entropy is higher for **1** (116.1 J mol^{-1} K^{-1}), followed by **5** (115.4 J mol^{-1} K^{-1}), **3** (114.2 J mol^{-1} K^{-1}), **2** (111.7 J mol^{-1} K^{-1}), and **4** (105.5 J mol^{-1} K^{-1}) (Table 3). On examination of the magnetic behavior of these compounds it is clear that the two $MePO_3^{2-}$ cages differ from the other cages. In the $\{Ni_6Y_6P_6\}$ cages, the

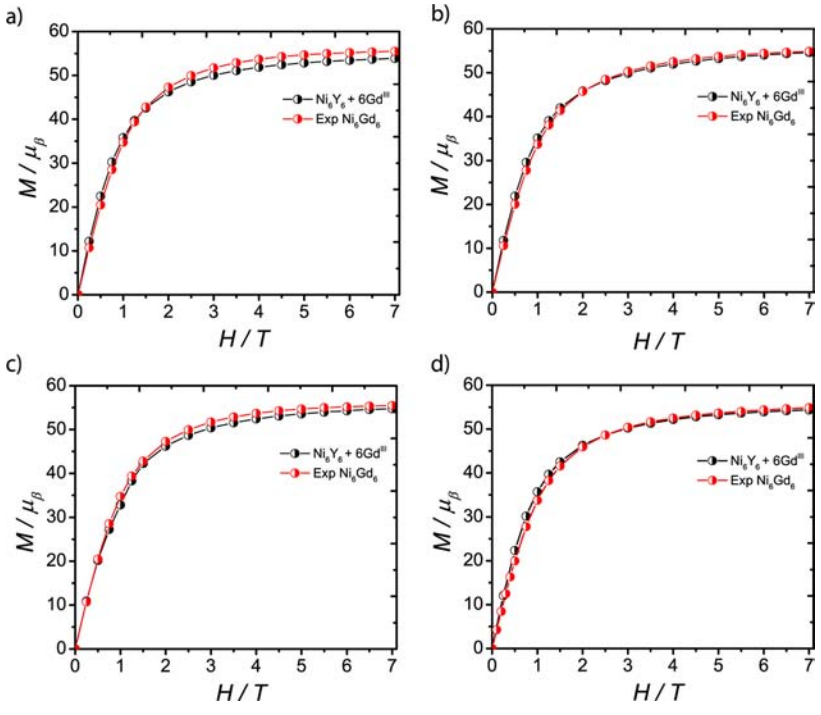

Figure 4. Comparison between experimental 2 K magnetization data for $\{Ni_6Gd_6P_6\}$ (red curves) and those for the analogous $\{Ni_6Y_6P_6\}$ cage plus the Brillouin function for six Gd^{III} ions (black curves): (a) cages **1** and **6**; (b) cages **3** and **7**; (c) cages **4** and **8**; (c) cages **5** and **9**.

dx.doi.org/10.1021/ic402296t | *Inorg. Chem.* 2013, 52, 13702−13707

Ni···Ni exchanges are found to be smaller in **6** in comparison with **7**−**9**, while in the $\{Ni_6Gd_6P_6\}$ cages there is evidence for ferromagnetic interactions in **1** and not in **3**−**5** (see Figure 4). A weak ferromagnetic interaction between Ni and Gd could explain the increase in magnetic entropy found in **1** being larger than would be predicted purely on molecular weight considerations. Ferromagnetic interactions are ideal for MCE, as these interactions allow saturation of the magnetization at lower magnetic fields; however, in order to allow faster demagnetization of the molecule after the removal of the applied field, weak ferromagnetic interactions are preferable.

The variations observed are very small, and there is a danger of making too much of a very subtle change: i.e., even if there is a Ni···Gd ferromagnetic exchange, it is barely observable. It does seem that $MePO_3^{2-}$ is subtly different from the other phosphonates, and perhaps this is due to the electron-releasing nature of the methyl group leading to greater electron density on the phosphonate and hence stronger superexchange.

CONCLUSIONS

A family of 3d−4f cages has been synthesized that resemble the Wells−Dawson ion. The structure seems insensitive to the phosphonate used. The magnetic entropy change of the cluster was improved through the reduction of the molecular mass using methylphosphonate; however, the increase seems slightly greater than would be expected if it were entirely due to mass change. Analysis of magnetization data suggests a weak ferromagnetic interaction between Gd and Ni, which could account for this difference.

The structural chemistry of phosphonate cages is intriguing. The coordinative flexibility of phosphonates allows the metal sites to adopt multiple different structures, and it is possible that the use of solvathermal methods favors a high-symmetry core in the structures. By regarding the P center as a "metal" center, we can describe this compound as akin to the Wells−Dawson ion. The question of whether there is a more general correlation between phosphonate cages and polyoxometalates is worth exploring. For example, while phosphonates support a $\{Ni_{12}\}$ cage containing a truncated tetrahedron similar to the Keggin ion,[13b] in that structure the P centers are not regarded as part of the polyhedron. Comparing the structures of these two extensive families of polymetallic cages might be instructive.

ASSOCIATED CONTENT

Supporting Information

Figures and CIF files giving crystallographic data, additional views of the crystal structures, a schematic of the bonding modes adopted by the ligands in the structure, and the magnetic measurements on all compounds. This material is available free of charge via the Internet at http://pubs.acs.org.

AUTHOR INFORMATION

Corresponding Authors

*E-mail for R.E.P.W.: richard.winpenny@manchester.ac.uk.

*E-mail for E.J.L.M.: eric.mcinnes@manchester.ac.uk.

Present Address

[†]Center for Applied Chemical Research, Frontier Institute of Science and Technology, Xi'an Jiaotong University, Xi'an 710054, People's Republic of China.

Notes

The authors declare no competing financial interest.

REFERENCES

(1) (a) Kahn, O. *Molecular Magnetism*; VCH: New York, 1993. (b) Gatteschi, D.; Sessoli, R.; Villain, J. *Molecular Nanomagnets*; Oxford University Press: Oxford, U.K., 2006.

(2) (a) Sessoli, R. *Angew. Chem., Int. Ed.* **2012**, *51*, 43. (b) Evangelisti, M.; Brechin, E. K. *Dalton Trans.* **2010**, *39*, 4672. (c) Evangelisti, M.; Candini, A.; Ghirri, A.; Affronte, M.; Brechin, E. K.; McInnes, E. J. L. *Appl. Phys. Lett.* **2005**, *87*, 072504. (d) Sharples, J. W.; Collison, D. *Polyhedron* **2013**, *54*, 91.

(3) (a) Karotsis, G.; Evangelisti, M.; Dalgarno, S. J.; Brechin, E. K. *Angew. Chem. int. Ed.* **2009**, *48*, 9928. (b) Langley, S. K.; Chilton, N. F.; Moubaraki, B.; Hooper, T. N.; Brechin, E. K.; Evangelisti, M.; Murray, K. S. *Chem. Sci.* **2011**, *50*, 6606. (c) Hooper, T. N.; Schnack, J.; Piligkos, S.; Evangelisti, M.; Brechin, E. K. *Angew. Chem., Int. Ed.* **2012**, *51*, 4633. (d) Zheng, Y.; Zhang, Q.-C.; Long, L.-S.; Huang, R.-B.; Müller, A.; Schnack, J.; Zheng, L.-S.; Zheng, Z. *Chem. Commun.* **2013**, *49*, 36.

(4) (a) Baskar, V.; Gopal, K.; Helliwell, M.; Tuna, F.; Wernsdorfer, W.; Winpenny, R. E. P. *Dalton Trans.* **2010**, *39*, 4747. (b) Wang, M.; Yuan, D.-Q.; Ma, C.-B.; Yuan, M.-J.; Hu, M.-Q.; Li, N.; Chen, H.; Chen, C.-N.; Liua, Q.-T. *Dalton Trans.* **2010**, *39*, 7276. (c) Zheng, Y.-Z.; Evangelisti, M.; Winpenny, R. E. P. *Angew. Chem., Int. Ed.* **2011**, *50*, 3692. (d) Zheng, Y.-Z.; Evangelisti, M.; Winpenny, R. E. P. *Chem. Sci.* **2011**, *2*, 99. (e) Zheng, Y.-Z.; Pineda, E. M.; Helliwell, M.; Evangelisti, M.; Winpenny, R. E. P. *Chem. Eur. J.* **2012**, *18*, 4161. (f) Zheng, Y.-Z.; Evangelisti, M.; Tuna, F.; Winpenny, R. E. P. *J. Am. Chem, Soc.* **2012**, *134*, 1057. (g) Pineda, E. M.; Tuna, F.; Zheng, Y.-Z.; Pritchard, R. G.; Regan, A. C.; Winpenny, R. E. P.; McInnes, E. J. L. *Chem. Commun.* **2013**, *49*, 3522.

(5) (a) Chaboussant, G.; Basler, R.; Güdel, H.-U.; Ochsenbein, S. T.; Parkin, A.; Parsons, S.; Rajaraman, G.; Sieber, A.; Smith, A. A.; Timco, G. A.; Winpenny, R. E. P. *Dalton Trans.* **2004**, 2758. (b) Aromi, G.; Batsanov, A. S.; Christian, P.; Helliwell, M.; Parkin, A.; Parsons, S.; Smith, A. A.; Timco, G. A.; Winpenny, R. E. P. *Chem. Eur. J.* **2003**, *9*, 5142.

(6) (a) Fomina, I. G.; Kiskin, M. A.; Martynov, A. G.; Aleksandrov, G. G.; Dobrokhotova, Z. V.; Gorbunova, Y. G.; Shvedenkov, Y. G.; Tsivadze, A. Y.; Novotortsev, V. M.; Eremenko, I. L. *Zh. Neorg. Khim.* **2004**, *49*, 1463. (b) Zoan, T. A.; Kuzmina, N. P.; Frolovskaya, S. N.; Rykov, A. N.; Mitrofanova, N. D.; Troyanov, S. I.; Pisarevsky, A. P.; Martynenko, L. I.; Korenev, Y. M. *J. Alloys Compd.* **1995**, *225*, 396.

(7) Dolomanov, O. V.; Bourthis, L. J.; Gildea, R. L.; Howard, J. A. K.; Puschmann, H. *J. Appl. Crystallogr.* **2009**, *42*, 339.

(8) Laye, R. H.; McInnes, E. J. L. *Eur. J. Inorg. Chem.* **2004**, *14*, 2811.

(9) Belsky, A. J.; Brill, T. B. *J. Phys. Chem. A* **1999**, *103*, 3006.

(10) Shaw, R.; Tidmarsh, I. S.; Laye, R. H.; Breeze, B.; Helliwell, M.; Brechin, E. K.; Heath, S. L.; Murrie, M.; Ochsenbein, S.; Güdel, H. U.; McInnes, E. J. L. *Chem. Commun.* **2004**, 1418.

(11) Chilton, N. F.; Anderson, R. P.; Turner, L. D.; Soncini, A.; Murray, K. S. *J. Comput. Chem.* **2013**, *34*, 1164.

(12) (a) Packov, A.; Miklovič, J.; Titiš, J.; Koman, M.; Boca, R. *Inorg. Chem. Commun.* **2013**, *32*, 9. (b) Charron, G.; Bellot, F.; Cisnetti, F.; Pelosi, G.; Rebilly, J.-N.; Riviere, E.; Barra, A.-L.; Mallah, T.; Policar, C. *Chem. Eur. J.* **2007**, *13*, 2774. (c) Boca, R. *Coord. Chem. Rev.* **2004**, *248*, 757.

(13) (a) $[Fe_{13}O_4F_{24}(OMe)_{12}]^{5-}$ reported in: Bino, A.; Ardon, M.; Lee, D.; Spingler, B.; Lippard, S. J. *J. Am. Chem. Soc.* **2002**, *124*, 4578. (b) $[Ni_{12}(OH)_4(O_3PPh)_4(O_2C^tBu)_{12}L_6]$, where L is a disordered mixture of solvents. See: Breeze, B. A.; Shanmugam, M.; Tuna, F.; Winpenny, R. E. P. *Chem. Commun.* **2007**, 5185.

(14) Coxall, R. A.; Harris, S. G.; Henderson, D. K.; Parsons, S.; Tasker, P. A.; Winpenny, R. E. P. *Dalton Trans.* **2000**, 2349.